THERMAL RESPONSE OF HEAT-RESISTANT LAYER WITH PYROLYSIS

by

Haiming HUANG*, Xiaoliang XU, Guo HUANG, and Zimao ZHANG

Institute of Engineering Mechanics, Beijing Jiaotong University, Beijing, China

Original scientific paper
DOI: 10.2298/TSCI110128035H

A model is developed for analyzing the thermal response of the heat-resistant layer composed of high silica fiber reinforced phenolic matrix composites (SiO_2/P) and aluminum, in which pyrolysis and phase transitions existed, such as melt, vaporization and sublimation. Based on this model, the thermal response of the heat-resistant layer with different SiO_2/P thickness is calculated under a heat flux by using FORTRAN codes. As indicated in the results, the slope of temperature gets a sudden decline at the pyrolysis interface, which is due to the latent heat of pyrolysis; the thickness of heat-resistant layer has little influence on the heating-surface temperature, however, the back temperature may increase with the decreasing thickness; and the thermal conductivity of carbonized layer is very important to thermal response.

Key words: *heat-resistant layer, pyrolysis, phase transition, thermal response*

Introduction

When a spacecraft flies in hypersonic speed, the kinetic energy is transferred into heat in ways of convection and radiation. Although being no more than one percent of the whole kinetic energy, the heat is still large enough to destroy the spacecraft. Generally, there are two approaches for protecting the spacecraft. One way is to optimize the flight trajectory so as to reduce the aerodynamic heating, and the other way is to exhaust the heat flux which is known as the thermal protection scheme [1].

Nowadays, three thermal protection schemes-heat sink, radiation, and ablation – can be used in heat design. However, with the increasing demand on the flying speed, a single scheme usually cannot fulfill the design requirements and the three thermal protection schemes should be used synthetically, so the actual thermal protection will be a complex process with thermal conduction, radiation, pyrolysis, and phase transition. On studies of the pyrolysis and phase transition, many achievements have been published, such as Ninković *et al*. [2] studied thermal and aerodynamic performances of supersonic motion, Alhama *et al*. [3] analyzed the rapid temperature changes in the composite nozzle wall by experimental methods, Huang *et al*. [4-6] presented a combined model for the flow past a blunt ablator and investigated the non-linear attributes of ablation and thermal contact resistance; Tong [7] gave

* Corresponding author; e-mail: hmhuang@bjtu.edu.cn

a qualitative model for simulating the tile gap heating on space shuttle; Mohammed *et al.* [8] calculated the transient response for different types of erodible surface thermocouples by using the finite element method, Bridgwater [9] studied the liquid bio-oil product from fast pyrolysis in transportable fuel, Vujić *et al.* [10] analyzed the influence of ambience temperature and operational-constructive parameters on landfill gas generation, Zheng *et al.* [11] studied flow and heat transfer of a power-law fluid over an unsteadily stretched surface by using a modified homotopy perturbation method, Chen *et al.* [12] investigated the entransy theory and its application to heat transfer in porous media, and Enzo *et al.* [13] studied the olive pits pyrolysis in a rotary kiln plant.

When the spacecraft is suffering high heat flux, pyrolysis and phase transitions result in the pyrolysis and phase transitions surfaces moving continuously, in another word, the ablation process corresponds to different thermal conduction model in different stages which are ignored in the classical ablation model. In this paper, the authors develop the ablation model for analyzing the thermal conduction of the heat-resistant layer, which is composed of aluminum and high silica fiber reinforced by phenolic matrix composites (SiO_2/P) with pyrolysis and phase transitions, such as melt, vaporization and sublimation, then calculate the thermal response of the heat-resistant layer with different SiO_2/P thickness, which may be helpful to the spacecraft design.

Model

SiO_2/P is a kind of reinforced composites with excellent attributes in heat insulation and ablation, which can be used as self-sudation material in aerospace field. As the heat flux along normal direction is far larger than that along other directions, the numerical model can be simplified as a 1-D model shown in fig.1. During the flight, the wall surface ($x = 0$) is heated continuously by the air with high compression ratio. The heat flux will be transferred along the x- axis and the ultimate target of thermal protection scheme is to assure the temperature of back surface ($x = x_5$) varies in a safe interval, so relative instruments can work safely under the cold structure layer; the phenolic resin begins to pyrolyze at 1020 K and the generated carbonized layer is constituted by carbon skeleton and silica in solid phase. Pyrolysis gas flows through the carbonized layer and takes some heat away. When the temperature increases to 2053 K, the solid silica begins to melt. When the temperature reaches 2500 K, the liquid silica boils and leaves the porous carbonized layer with low strength and may be easily washed away.

Before simulations are carried out, three assumptions are presented as:

– the oxidation of carbon is neglected, which means, $x_1 = 0$,
– thermo-physical attributes of silica can be seen as invariant, that is:

$$\rho_{\mathrm{SiO_2(L)}} = \rho_{\mathrm{SiO_2}(S)}, \quad k_{\mathrm{SiO_2(L)}} = k_{\mathrm{SiO_2(S)}}, \quad c_{p,\mathrm{SiO_2(L)}} = c_{p,\mathrm{SiO_2(S)}} \tag{1}$$

– the density and specific heat of carbonized layer are:

$$\rho_{\mathrm{SiO_2/C}} = \rho_{\mathrm{SiO_2}}\phi_{\mathrm{SiO_2}} + \rho_{\mathrm{C}}\phi_{\mathrm{C}} \tag{2}$$

$$c_{P,\mathrm{SiO_2/C}} = c_{P,\mathrm{SiO_2}}\phi_{\mathrm{SiO_2}} + c_{P,\mathrm{C}}\phi_{\mathrm{C}} \tag{3}$$

In the thermal response model shown in fig. 1, there are five possible cases which are:

Case 1: while $T_{max} \le 1020$ K, the model is constituted by aluminum and SiO_2/P, namely, $x_2 = x_3 = 0$.

The heat conduction equation in the two layers can be written as:

$$\rho_{Al} c_{P,Al} \frac{\partial T}{\partial t} = k_{Al} \frac{\partial^2 T}{\partial x} \tag{4}$$

and

$$\rho_{SiO_2/P} c_{P,SiO_2/P} \frac{\partial T}{\partial t} = k_{SiO_2/P} \frac{\partial^2 T}{\partial x} \tag{5}$$

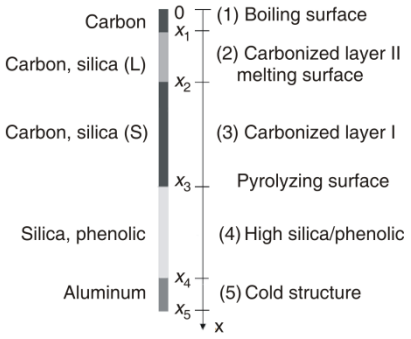

Figure 1. Thermal response of the heat resistant layer

Case 2: while 1020 K $\le T_{max} \le$ 2053 K and $T_{min} \le 1020$ K, the model adopts three layers: aluminum, SiO_2/P, and the carbonized layer I, namely, $x_2 = 0$.

The heat conduction equation in the three layers can be:

$$\rho_{Al} c_{P,Al} \frac{\partial T}{\partial t} = k_{Al} \frac{\partial^2 T}{\partial x} \tag{6}$$

$$\rho_{SiO_2/P} c_{P,SiO_2/P} \frac{\partial T}{\partial t} = k_{SiO_2/P} \frac{\partial^2 T}{\partial x} \tag{7}$$

$$\rho_{SiO_2(S)/C} c_{P,SiO_2(S)/C} \frac{\partial T}{\partial t} = k_{SiO_2(S)/C} \frac{\partial^2 T}{\partial x^2} + \dot{m}_p c_{P,g} \frac{\partial T}{\partial x} \tag{8}$$

Case 3: while 2053 K < $T_{max} \le$ 2500 K and $T_{min} \le 1020$ K, the model is constituted by aluminum, SiO_2/P, the carbonized layers I and II, namely $x_2 = 0$.

The heat conduction equation in these four layer are:

$$\rho_{Al} c_{P,Al} \frac{\partial T}{\partial t} = k_{Al} \frac{\partial^2 T}{\partial x} \tag{9}$$

$$\rho_{SiO_2/P} c_{P,SiO_2/P} \frac{\partial T}{\partial t} = k_{SiO_2/P} \frac{\partial^2 T}{\partial x} \tag{10}$$

$$\rho_{SiO_2(S)/C} c_{P,SiO_2(S)/C} \frac{\partial T}{\partial t} = k_{SiO_2(S)/C} \frac{\partial^2 T}{\partial x^2} + \dot{m}_p c_{P,g} \frac{\partial T}{\partial x} \tag{11}$$

$$\rho_{SiO_2(L)/C} c_{P,SiO_2(L)/C} \frac{\partial T}{\partial t} = k_{SiO_2(L)/C} \frac{\partial^2 T}{\partial x^2} + \dot{m}_p c_{P,g} \frac{\partial T}{\partial x} + \dot{m}_r c_{P,SiO_2(L)} \frac{\partial T}{\partial x} \tag{12}$$

Case 4: while $T_{max} > 2500$ K and $T_{min} > 1020$ K, the model is make up of aluminum, carbonized layer I and II, namely $x_3 = x_4 = x_5$.

Case 5: while $T_{max} > 2500$ K, the model contains two layers: aluminum and the carbonized layer II, namely $x_2 = x_3 = x_4 = x_5$.

In cases 4 and 5, aluminum must have been molten and the support structure fails, when SiO_2/P is completely pyrolyzed, the calculation makes no sense.

The boundary conditions on wall surface, back surface, and the interfaces among layers can be written as:

$$-k_{\mathrm{SiO_2(L)/C}}\frac{\partial T(x,t)}{\partial x} = q_{\mathrm{w}} - \varepsilon\sigma T_{\mathrm{w}}^4 \qquad (x = 0) \tag{13}$$

$$-k_{\mathrm{SiO_2(S)/C}}\frac{\partial T(x,t)}{\partial x} = -k_{\mathrm{SiO_2(L)/C}}\frac{\partial T(x,t)}{\partial x} + \dot{m}_{\mathrm{r}}\Delta H_{\mathrm{r}} \qquad (x = x_2) \tag{14}$$

$$-k_{\mathrm{SiO_2/P}}\frac{\partial T(x,t)}{\partial x} = -k_{\mathrm{SiO_2(S)/C}}\frac{\partial T(x,t)}{\partial x} + \dot{m}_{\mathrm{p}}\Delta H_{\mathrm{p}} \qquad (x = x_3) \tag{15}$$

$$-k_{\mathrm{SiO_2/P}}\frac{\partial T(x,t)}{\partial x} = -k_{\mathrm{Al}}\frac{\partial T(x,t)}{\partial x} \qquad (x = x_4) \tag{16}$$

$$\frac{\partial T(x,t)}{\partial x} = 0 \qquad (x = x_5) \tag{17}$$

The heat conduction equations can be solved by using the pursuit method in a difference scheme. Take case 3 for example, the discrete scheme of eq. (12) can be written as:

$$\rho_{\mathrm{S_iO_2(L)/C}}c_{P,\mathrm{SiO_2(L)/C}}\frac{T_j^{(n)} - T_j^{(n-1)}}{\Delta t} = k_{\mathrm{SiO_2(L)/C}}\frac{T_{j+1}^{(n)} - 2T_j^{(n)} + T_{j-1}^{(n)}}{\Delta x_2{}^2} + \\ + \dot{m}_{\mathrm{p}}c_{P,\mathrm{g}}\frac{T_j^{(n)} - T_j^{(n-1)}}{\Delta x_2} + \dot{m}_{\mathrm{r}}c_{P,\mathrm{SiO_2(L)}}\frac{T_j^{(n)} - T_j^{(n-1)}}{\Delta x_2} \tag{18}$$

which is

$$1 + 2r_2\ \ T_j^{(n)} = \ r_2 + z_2\ \ T_{j+1}^{(n)} + \ r_2 - z_2\ \ T_{j-1}^{(n)} + T_j^{(n-1)} \tag{19}$$

where $r_2 = \dfrac{k_{\mathrm{SiO_2(L)/C}}\Delta t}{\rho_{\mathrm{SiO_2(L)/C}}c_{P,\mathrm{SiO_2(L)/C}}(\Delta x_2)^2}$ and $z_2 = \dfrac{(\dot{m}_{\mathrm{p}}c_{\mathrm{p,g}} + \dot{m}_{\mathrm{r}}c_{P,\mathrm{SiO_2(L)}})\Delta t}{2\rho_{\mathrm{SiO_2(L)/C}}c_{P,\mathrm{SiO_2(L)/C}}\Delta x_2}$

Denote $A_2 = 1 + 2r_2$, $B_2 = r_2 + z_2$, $C_2 = r_2 - z_2$, $D_2 = T_j^{(n-1)}$, and eq. (19) becomes:

$$A_2T_j^{(n)} = B_2T_{j+1}^{(n)} + C_2T_{j-1}^{(n)} + D_2 \tag{20}$$

Similarly, discrete scheme of other layers can be written as:

$$A_iT_j^{(n)} = B_iT_{j+1}^{(n)} + C_iT_{j-1}^{(n)} + D_i \quad (i = 2, 3, 4, 5) \tag{21}$$

Eliminate $T_{j+1}^{(n)}$, eq. (21) becomes:

$$T_{j-1}^{(n)} = P_{j-1}^{(n)} T_j^{(n)} + Q_{j-1}^{(n)} \tag{22}$$

where
$$P_j^{(n)} = \frac{B_j^{(n)}}{A_j^{(n)} - C_j^{(n)} P_{j-1}^{(n)}}, \quad Q_j^{(n)} = \frac{D_j^{(n)} + C_j^{(n)} Q_{j-1}^{(n)}}{A_j^{(n)} - C_j^{(n)} P_{j-1}^{(n)}} \tag{23}$$

From the thermal insulation eq. (17) we know $T_1^{(n)} = T_2^{(n)}$, that is $P_1^{(n)} = 1$ and $Q_1^{(n)} = 0$. Denoting the numbers of elements in each layer are, respectively, M_2, M_3, M_4, and M_5, and the boundary eq. (16) becomes:

$$-k_{\mathrm{Al}} \frac{T_{\mathrm{M}_5+1}^n - T_{\mathrm{M}_5}^n}{\Delta x_5} = -k_{\mathrm{SiO_2/P}} \frac{T_{\mathrm{M}_5+2}^n - T_{\mathrm{M}_5+1}^n}{\Delta x_4} \tag{24}$$

Put the equation:

$$T_{\mathrm{M}_5}^{(n)} = P_{\mathrm{M}_5}^{(n)} T_{\mathrm{M}_5+1}^{(n)} + Q_{\mathrm{M}_5}^{(n)} \tag{25}$$

into eq. (24), we get:

$$T_{\mathrm{M}_5+1}^{(n)} = P_{\mathrm{M}_5+1}^{(n)} T_{\mathrm{M}_5+2}^{(n)} + Q_{\mathrm{M}_5+1}^{(n)} \tag{26}$$

where
$$P_{\mathrm{M}_5+1}^{(n)} = \frac{1}{\frac{k_{\mathrm{Al}} \Delta x_4}{k_{\mathrm{SiO_2/P}} \Delta x_5} (1 - P_{\mathrm{M}_5}^{(n)}) + 1}, \quad Q_{\mathrm{M}_5+1}^{(n)} = \frac{Q_{\mathrm{M}_5}^{(n)}}{(1 - P_{\mathrm{M}_5}^{(n)}) + \frac{k_{\mathrm{SiO_2/P}} \Delta x_5}{k_{\mathrm{Al}} \Delta x_4}}$$

Similarly, we obtain:

$$P_{\mathrm{M}_5+\mathrm{M}_4+1}^{(n)} = \frac{1}{\frac{k_{\mathrm{SiO_2/P}} \Delta x_3}{k_{\mathrm{SiO_2(S)/C}} \Delta x_4} (1 - P_{\mathrm{M}_5+\mathrm{M}_4}^{(n)}) + 1}, \quad Q_{\mathrm{M}_5+\mathrm{M}_4+1}^{(n)} = \frac{Q_{\mathrm{M}_5+\mathrm{M}_4}^{(n)} - \dot{m}_{\mathrm{p}} \Delta H_{\mathrm{p}}}{(1 - P_{\mathrm{M}_5+\mathrm{M}_4}^{(n)}) + \frac{k_{\mathrm{SiO_2(S)/C}} \Delta x_4}{k_{\mathrm{SiO_2/P}} \Delta x_3}}$$

$$P_{\mathrm{M}_5+\mathrm{M}_4+\mathrm{M}_3+1}^{(n)} = \frac{1}{\frac{k_{\mathrm{SiO_2(S)/C}} \Delta x_2}{k_{\mathrm{SiO_2(L)/C}} \Delta x_3} (1 - P_{\mathrm{M}_5+\mathrm{M}_4+\mathrm{M}_3}^{(n)}) + 1}, \quad Q_{\mathrm{M}_5+\mathrm{M}_4+\mathrm{M}_3+1}^{(n)} = \frac{Q_{M_5+M_4+M_3}^{(n)} - \dot{m}_{\mathrm{r}} \Delta H_{\mathrm{r}}}{(1 - P_{\mathrm{M}_5+\mathrm{M}_4+\mathrm{M}_3}^{(n)}) + \frac{k_{\mathrm{SiO_2(L)/C}} \Delta x_3}{k_{\mathrm{SiO_2(S)/C}} \Delta x_2}}$$

From eq. (13) we have:

$$-k_{\mathrm{SiO_2(L)/C}} \frac{T_{\mathrm{M}_5+\mathrm{M}_4+\mathrm{M}_3+\mathrm{M}_2+1} - T_{\mathrm{M}_5+\mathrm{M}_4+\mathrm{M}_3+\mathrm{M}_2}}{\Delta x_2} = q_w - \varepsilon\sigma T_{\mathrm{M}_5+\mathrm{M}_4+\mathrm{M}_3+\mathrm{M}_2+1}^4 \tag{27}$$

put $T_{\mathrm{M}_5+\mathrm{M}_4+\mathrm{M}_3+\mathrm{M}_2}^{(n)} = P_{\mathrm{M}_5+\mathrm{M}_4+\mathrm{M}_3+\mathrm{M}_2}^{(n)} T_{\mathrm{M}_5+\mathrm{M}_4+\mathrm{M}_3+\mathrm{M}_2+1}^{(n)} + Q_{\mathrm{M}_5+\mathrm{M}_4+\mathrm{M}_3+\mathrm{M}_2}^{(n)}$ into eq. (27), and we get:

$$-k_{\mathrm{SiO_2(L)/C}} \frac{(1 - P_{\mathrm{M}_5+\mathrm{M}_4+\mathrm{M}_3+\mathrm{M}_2}^{(n)}) T_{\mathrm{M}_5+\mathrm{M}_4+\mathrm{M}_3+\mathrm{M}_2+1}^{(n)} - Q_{\mathrm{M}_5+\mathrm{M}_4+\mathrm{M}_3+\mathrm{M}_2}^{(n)}}{\Delta x_2} = q_{\mathrm{w}} - \varepsilon\sigma T_{\mathrm{M}_5+\mathrm{M}_4+\mathrm{M}_3+\mathrm{M}_2+1}^4 \tag{28}$$

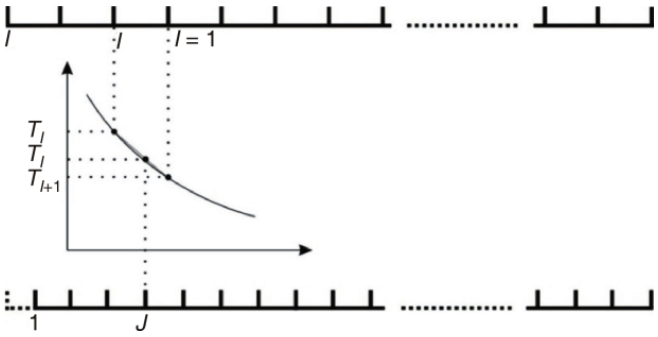

Figure 2. Re-division of ablation grids and interpolation of nodes data

By solving the non-linear eq. (28), we can obtain $T^{(n)}_{M_5+M_4+M_3+M_2+1}$, and then the thermal response of the whole heat resistant layer can be calculated by using Thomas method based on Gauss elimination. As is shown in fig. 2, the boundary is moving continuously, the grid should be re-divised before a new round of calculation, and the temperature on a new grid node may be calculated from the old grid by interpolation.

An example

The radiation coefficient takes 0.8 and the initial temperature is 300 K. The aluminum layer is 4 mm thick, $\rho_{A1} = 2643$ kg/m^3, $k_{A1} = 249.1$ W/mK, $c_{P,Al} = 1.089$ kJ/kgK, and $\alpha_{Al} = = 0.865\cdot10^{-6}$ m^2/s, the thickness of SiO_2/P layer are 21, 23, or 25 mm, respectively; $\rho_{SiO_2/P} = = 1700$ kg/m^3, $k_{SiO_2/P} = 0.65$ W/mK, $c_{P,SiO_2/P} = 1.20$ kJkg/K, and $\rho_{SiO_2/P} = 0.319\cdot10^{-6}$ m^2/s.

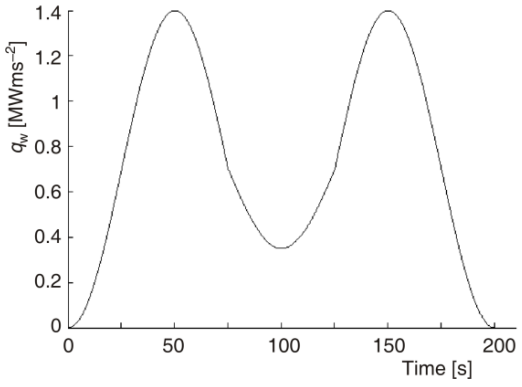

Figure 3. Aerodynamic heat flux on the supersonic spacecraft

In fig. 3, we plot a curve of aerodynamic heat flux exerted on a flying spacecraft for 200 seconds according to our flying experiment, which is relevant to some military need in China. From the measured radiation heat flux shown in fig. 4, we inverse the development of actual heating-surface temperature and plot it in fig. 5. The actual thermal conductivity of carbonized layer is very difficult to obtain, however, it may have a great influence on heating-surface temperature, back temperature, distribution of temperature, and heat flux, so we solve the heat conduction equation with different assumed thermal conductivity, and then compare the calculated heating-surface temperature with the experimental data in order to find the most possible thermal conductivity.

The temperature calculated under different k_{cl} is shown in fig. 6: the larger k_{cl} corresponding to the higher back temperature and the thicker carbonized layer. When the thermal conductivity of SiO_2/P is smaller and k_{cl} is relatively larger, the heat accumulates at the interface between SiO_2/P and carbonized layer so that the pyrolysis surface put forward very fast and the back temperature be much higher; otherwise, when k_{cl} is relatively smaller, the back temperature will be lower and the carbonized layer is thinner. So the thermal conductivity is very important.

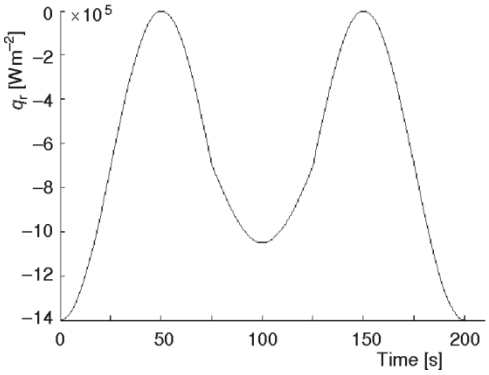

Figure 4. Radiation heat flux on spacecraft surface

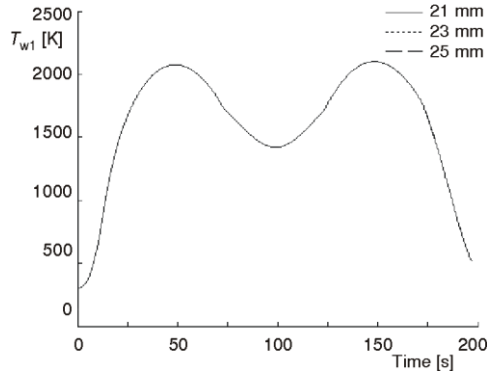

Figure 5. Heating-surface temperature inversed from radiation heat flux

The heating-surface temperature (Tw_1) and back temperature (Tw_o) calculated with different k_{cl} (0.75, 3.0, 4.5, and 7.5 W/mK) are shown in fig. 7 and 8, respectively. With a comparison between the development of heating-surface temperature and the experimental one shown in fig. 5, we known the two curves get the best match at k_{cl} = 0.75 Wm/K, which is close to the true data.

When k_{cl} = 0.75 W/mK and SiO_2/P layer is 2, 23 or 25 mm thick, we calculate the development of heating-surface and back temperature. As is shown in fig. 9,

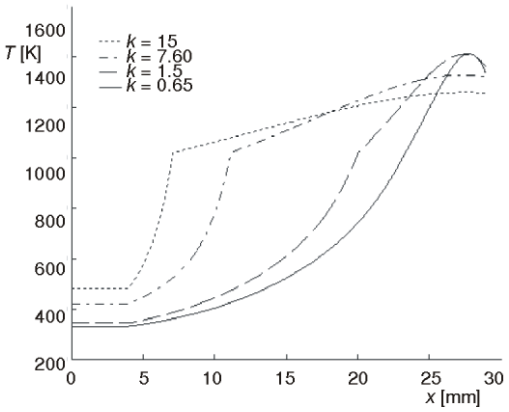

Figure 6. k_{cl} influence on temperature

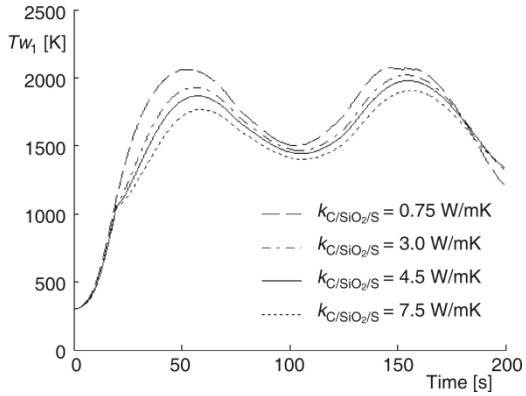

Figure 7. Heating-surface temperature calculated from different k_{cl} ($\delta_{SiO_2/P}$ = 21 mm)

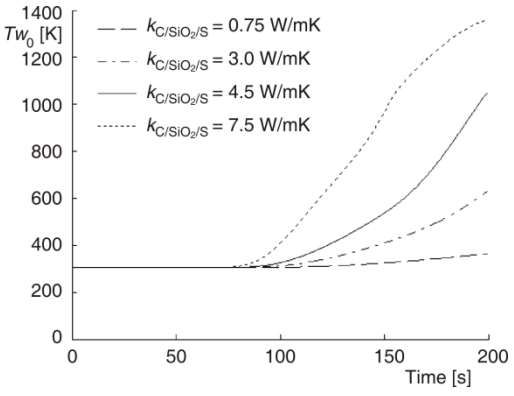

Figure 8. Back temperature calculated from different k_{cl} ($\delta_{SiO_2/P}$ = 21 mm)

there is little difference on the heating-surface temperature, which agrees with the experimental case shown in fig. 5. As can be seen in fig. 10, the maximum back temperature 372 K corresponds to the least thickness of $l_{SiO_2/P}$, whereas the minimum back temperature 323 K corresponds to the largest $l_{SiO_2/P}$.

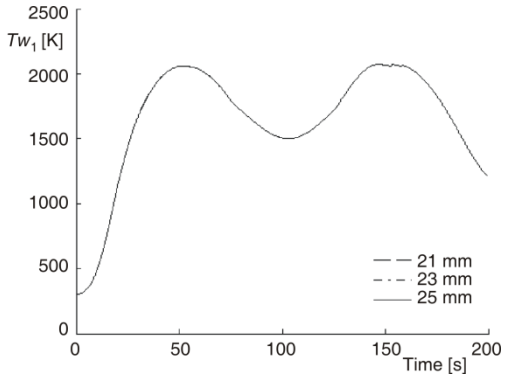

Figure 9. Development of heating-surface temperature with different $l_{SiO_2/P}$, (k_{cl} = 0.75 W/mk)

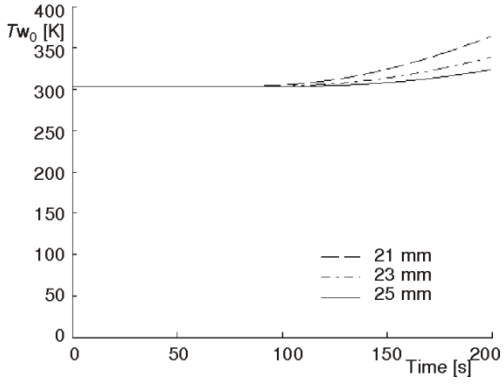

Figure 10. Development of back temperature with different $l_{SiO_2/P}$, (k_{cl} = 0.75 W/mk)

The distributions of temperature and heat flux at t = 200 s are shown in fig. 11 and fig. 12, respectively. The temperature is relatively uniform in the aluminum layer, as the thermal conductivity of aluminum is much larger than SiO_2/P; the slope of temperature gets a sudden decline at T = 1020 K, which is due to the heat absorption of pyrolysis, and the maximum heat flux appears at the pyrolytic interface T = 1020 K (shown in fig. 12).

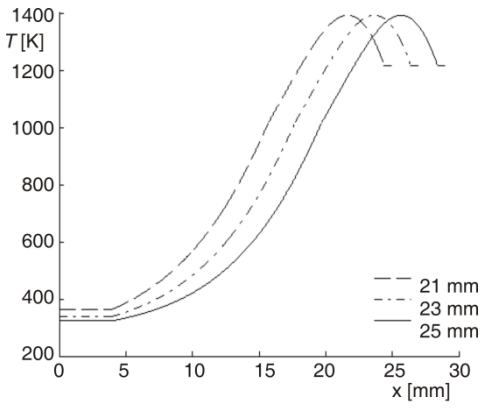

Figure 11. Temperature at T = 200 s of different $l_{SiO_2/P}$ (k_{cl} = 0.75 Wm/K)

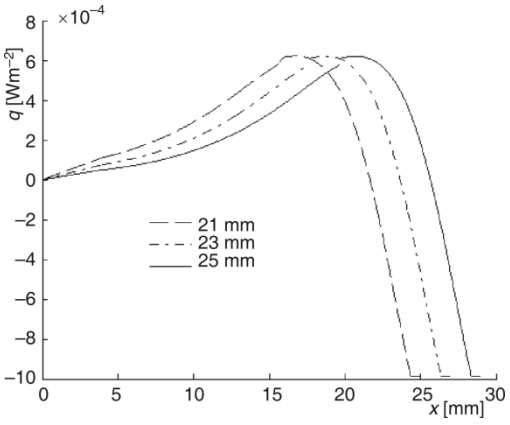

Figure 12. Heat flux at T = 200 s of different $l_{SiO_2/P}$ (k_{cl} = 0.75 $Wm^{-1}K^{-1}$)

Conclusions

In this paper, we present a model for studying thermal response of the heat resistant layer which is constituted by aluminum and SiO_2/P. In this model, pyrolysis is considered as

well as phase transitions such as melt, vaporization, and sublimation. On the basis of this model, we calculate the thermal response of aluminum layer and different thickness of SiO_2/P under an experimental heat flux. The slope of temperature gets a sudden decline at pyrolysis interface, which is due to the latent heat of pyrolysis; the thickness of heat-resistant layer has little influence on heating-surface temperature, however, with the thickness decreasing, the back temperature may increase; the thermal conductivity of carbonized layer has a great influence on thermal response. This study may afford some advice to spacecraft design.

Acknowledgment

This work was supported by the National Natural Sciences Foundation of China (No. 10572020), the Fundametnal Research Funds for the Central Universities and Grant Research of China (No. 61391).

Nomenclature

c_P – specific heat, [kJkg^{-1}K^{-1}]
ΔH_p – latent heat of pyrolysis, [MJkg^{-1}]
ΔH_r – latent heat of melt, [MJkg^{-1}]
k – thermal conductivity, [Wm^{-1}K^{-1}]
k_{cl} – thermal conductivity of carbonized layer, [Wm^{-1}K^{-1}]
l – thickness, [m]
$\dot{m}_p$ – mass change rate of pyrolysis, [ms^{-1}]
$\dot{m}_r$ – mass change rate of melt, [ms^{-1}]
q_w – heat flow on the wall, [Wm^{-2}]
T – temperature, [K]

Greeks symbols

α – thermal diffusivity, [m^{2}s^{-1}]
ε – radiation factor of the wall, [–]
ρ – density, [kgm^{-3}]
σ – Stefan-Boltzmann constant, [Wm^{-2}K^{-4}]
ϕ – volume fraction, [–]

References

[1] Huang, H. M., Xu, X. L., Jiang, G. Q. Discrimination for Ablative Control Mechanism in Solid-Propellant Rocket Nozzle, *Science in China Series E, 52* (2009), 10, pp. 2911-2917
[2] Ninković, D. P., Thermal and Aerodynamic Performances of the Supersonic Motion, *Thermal Science, 14* (2010), 4, pp. 1089-1100
[3] Alhama, F., Campo, A. Network Simulation of the Rapid Temperature Changes in the Composite Nozzle Wall of An Experimental Rocket Engine During a Ground Firing Test, *Applied Thermal Engineering, 23* (2003), 1, pp. 37-47
[4] Huang, H. M., *et al*., Nonlinear Analysis of Flow Past a Blunt Ablator, Part I: Combined Numerical Model, *International Journal of Nonlinear Science and Numerical Simulation, 11* (2010), 7, pp. 543-552
[5] Xu, X. L., Huang, H. M., Jiao, W., Nonlinear Analysis of Flow Past Blunt Ablator, II Simulation and Chaos Identification, *International Journal of Nonlinear Sciences and Numerical Simulation, 11* (2010) 7, pp. 553-561
[6] Huang, H. M., Xu, X. L. Effects of Surface Morphology on Thermal Contact Resistance, *Thermal Science, 15* (2011), Suppl. 1, pp. S33-S38
[7] Tong, B. G. A Qualitative Study of Tile Gap Heating on Space Shuttle, *Aerodynamic Experiment and Measurement and Control, 4* (1999), 4, pp. 1-8
[8] Mohammed, H., Salleh, H., Yusoff, M. Z., The Transient Response for Different Types of Erodable Surface Thermocouples Using Finite Element Analysis, *Thermal Science, 11* (2007), 4, pp. 49-64
[9] Bridgwater, A. V., Biomass Fast Pyrolysis, *Thermal Science, 8* (2004) 2, pp. 21-49
[10] Vujić, G., *et al*., Influence of Ambience Temperature and Operational-Constructive Parameters on Landfill Gas Generation, *Thermal Science, 14* (2010) 2, pp. 555-564

[11] Zheng, L. C., *et al*., Analyzing the Flow and Heat Transfer of a Power-Law Fluid over an Unsteadily Atretched Aurface Using A Modified Homotopy Perturbation Method, *International Journal of Nonlinear Science and Numerical Simulation, 11* (2010) 10, pp. 843-849
[12] Chen, Q., Guo, Z. Y. Entransy Theory and Its Application to Heat Transfer Analyses in Porous Media, *International Journal of Nonlinear Science and Numerical Simulation, 11* (2010) 1, pp. 11-22
[13] Benanti, E., *et al*., Simulation of Olive Pits Pyrolysis in a Rotary Kiln Plant, *Thermal Science, 15* (2011), 1, pp. 145-158

Paper submitted: January 28, 2011
Paper revised: May 6, 2011
Paper accepted: May 7, 2011